



Detection of Gallbladder Disorder through Iris Using Deep Learning Models for Classification

M. SANDHIYA

Research Scholar, Department of Computer Science, VELS Institute of Science, Technology & Advanced Studies (VISTAS),

Chennai – 117 sandyamano.10@gmail.com

Dr. A.S. ANEETHA

Associate Professor, Department of Computer Science, VELS Institute of Science, Technology & Advanced Studies (VISTAS), Chennai-117 aneetha.scs@velsuniv.ac.in

Abstract

An analysis of the distinct patterns present in the iris enables the identification of possible markers of gallbladder problems via the application of deep learning. Deep learning techniques are a dependable and quickly developing field for diagnosing disorders, as demonstrated by biomedical research. This study uses human iris to assess the diagnostic accuracy of iridology for gallbladder issues. The training dataset consists of 2481 images belonging to two classes with normal and abnormal gallbladder was used in the study. The iris images, each measuring 640 by 480 pixels, were taken. Using the iridology chart as a reference, the focal area in the iris image was chosen so that it matched the location of the specific organ. Then, using statistical analysis features and the 2D Discrete Wavelet Transform (DWT), characteristics from this region features were extracted. The results demonstrate that the classifier generated the highest classification accuracy by using ResNet-50. It has been demonstrated that the suggested model for the automatic and non-invasive detection of gallbladder disorders is both diagnostically significant and effective.

Keywords: Iris, gallbladder disorder, segmentation, feature extraction, classification, disorder detection.

Introduction

Recently, there have been new opportunities for disease detection and classification due to the convergence of artificial intelligence (AI) and medical diagnostics. The utilization of iris pictures for health-related diagnostics is one field that has attracted attention because of the useful information that their unique patterns hold (Tania Weidan Yu EECS, 2018). The analysis of iris pictures for the purpose of diagnosing gallbladder problems is the specific focus of this research. Advanced deep learning models are used to obtain accurate classification. Gallbladder disorders, encompassing ailments such as inflammation, gallstones, and anomalies in function, represent a significant global public health concern (Lam et al., 2021). Accurate and quick diagnosis of these illnesses is essential to enable appropriate intervention and improve patient outcomes. The deep learning algorithm looks for patterns in the iris that are specific to conditions like gallbladder diseases and other systemic health problems. By scans of iris from patients with established gallbladder diseases and a healthy control group, the model was trained. This research advances the field of medical image processing and offers non-invasive diagnostic techniques to enhance healthcare procedures ((Alghazo & Latif, 2023) this study's findings may contribute to better early detection techniques and gallbladder disorder information management.

Literature review

In particular, the assessment of the literature highlights the increasing amount of research that focuses on gallbladder problems and examines iris recognition systems for medical diagnosis. The results show that iris-based methods can be non-invasive and successful, and they open the door to the use of deep learning models to improve the efficiency and accuracy of gallbladder health diagnosis. From a series of intra-abdominal ultrasound images, they utilize DNN to identify the organ, then they use the form and texture qualities to identify GB anomalies. The suggested AI system can be expanded and used for many additional bodily systems and diseases by compiling thorough data about a greater number of people with diverse ailments (Obaid et al., 2023) the possibility of diagnosing liver diseases and categorizing diabetes using iris mapping and texture information taken from iris photos. (Hussein et al., 2013; Samant & Agarwal, 2018b) A useful method for clinical diagnosis is iris image analysis, especially in iridodiagnosis, where different diseases can be identified using iris mapping and texture properties. an effective machine learning method for nephrology using iris recognition, which evaluates the color, patterns, and characteristics of the iris to identify organ diseases and determine a person's overall health (Divya et al., 2021). Specific parts of the iris were used to extract various properties, such as statistical characteristics, features based on a gray-level co-occurrence matrix, and features based on a gray-level run length matrix. This might be used as a non-invasive, contactless way to diagnose diabetes and provide information on how common

the condition is and how long it lasts. Using the designated regions shown in the iridology chart, pre-image processing techniques were used to extract the region of interest from the iris. A subsequent study was carried out to assess the first-order statistical and second-order textual properties of the extracted region of interest. (Jensen, 1980). Both radial and angular orientations can be used to compute statistical features. Improving the angular or radial resolution in addition to normalization improves iris detection accuracy. A 200-bit feature vector is appropriate for statistical feature extraction along the radial direction, according to empirical studies with varying resolutions, and a 1000-bit feature vector is ideal for statistical feature extraction along the angular direction, yielding an excellent iris performance (Bansal et al., 2016). This research could be extended to include a wider range of diseases, leading to the development of computer-aided diagnosis tools that are easy to use and can support people in preserving their health. Furthermore, complementary and alternative medicine holds potential in diagnosing problems associated with gastrointestinal disorders (Carrera & Maya, 2019). A CNN-based system for the non-invasive detection of diabetes mellitus was developed using the iridology approach. Segmentation and ROI selection were removed from the system's classification process (Velia & Saputro, 2020). It provides important insights into the efficacy of machine learning methods and iris image analysis for diabetes diagnosis utilizing iris images through a comparative comparison of classification-based algorithms (Samant & Agarwal, 2018a) the effectiveness of ConvNet models that have already been trained and investigates the impact of retraining and data augmentation methods. These assessments provide important information about the possibility of achieving high iris recognition accuracy rates (Yow & Ali, 2019). Iris images are produced by applying wavelet analysis to the 3D structure of the iris muscle. This approach uses SVM kernels and the Gabor filter to extract and classify features. Its performance is compared to other approaches to show how it may be used to increase the security of iris recognition systems (Lee & Park, 2010). To increase the robustness of the segmentation performance, we used ResNet-50 in place of the original network in the network contracting path (Wei et al., 2022) to explore the possibilities of using iris images for human organ disorder detection. Here, we present a Deep Learning model-based method for identifying gallbladder regions from iris image.

Methodology and model specifications

The new methodology proposes diagnostic techniques by providing a non-invasive means of evaluating each person's gallbladder condition and identifying any essential safety measures. Many pre-processing techniques were tried with captured images for iris localization and segmentation algorithms in this study. Figure 1 shows the fundamental procedures used in the study. The following subsections offer a succinct overview of these phases.

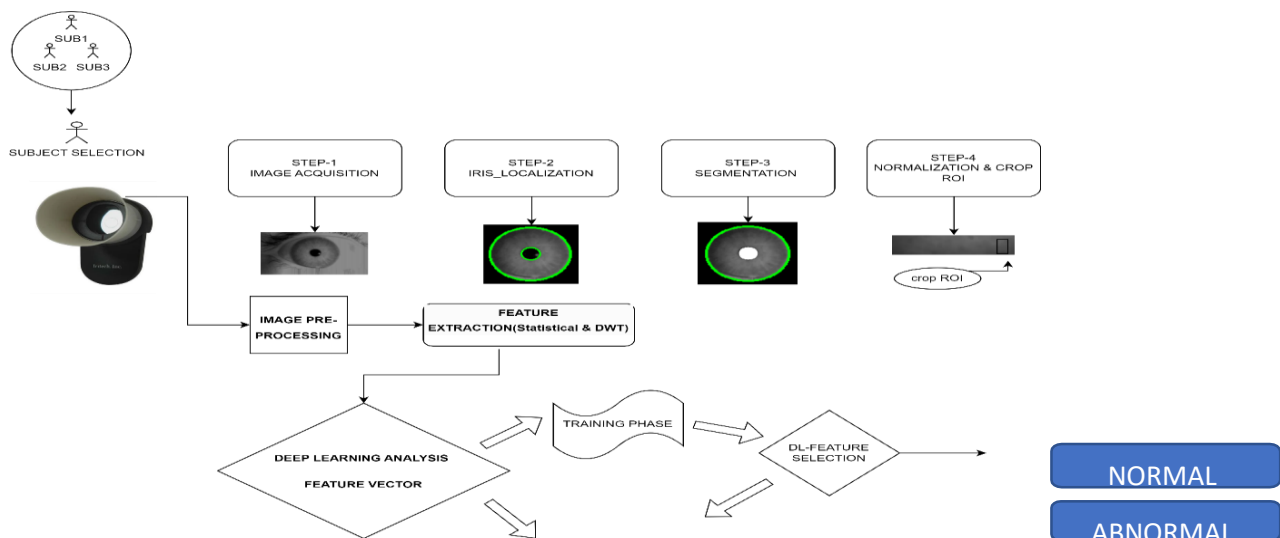


Fig-1: Proposed Methodology

Enrollment of Participants and Image Collection

A specific iris technology camera is used to capture images in the examination of gallbladder problem detection by Iris. This camera, which is intended exclusively for biometric applications, is an essential component of the research. It has special characteristics that are tailored to take only excellent right iris pictures for additional examination (IriShield™ MK2120UL, 2021) Fig-2.



Capture Mode	Auto capture with built-in quality check (using NIST IQCE and ISO 29794-6 quality metrics)
Key Functionalities	On-board Template Generation, 1:1 and 1:N Template Matching On-board PKI security functions
Viewfinder	Capture distance: 14 - 15 cm (5.5 - 5.9 in) Capture volume: 33 x 24 x 10 mm
Image Format	ISO 18794-6, full support of K1, K2, K3, and K7 Max 640 x 480 pixels, 8-bit grayscale
Sensor	Resolution: VGA, Scan type: Progressive, SNR: > 37 dB
Pixel Density	Normally greater than 210 pixels across iris diameter

Fig-2: Irishield™ Mk2120ul

Iris preprocessing

(a). *Noise Reduction*: The reflective noise removal operation (Yu et al., 2021) can be expressed in a pseudo-mathematical form.

$$RNR(I[i, j]) = \begin{cases} B_{uff} & \text{if } I[i, j] > T_1 \\ I[i, j] & \text{otherwise} \end{cases}$$

The grayscale input image is taken as an input by the algorithm. The algorithm requires four parameters, namely L_c , R_c , U_r , and D_r , which define a region of interest within the image where the reflective noise reduction will be applied. These parameters should be adjusted based on the characteristics of the input images. The reflective_noise_removal function performs several steps, including calculating the average grayscale value of the entire image (T_1), initializing a buffer (B_{uff}) with the average grayscale value, and iterating through the region of interest. For each pixel in the specified region of interest, if the pixel value is greater than the average grayscale value (T_1), the pixel value is set to the buffer value (B_{uff}). If the pixel value is less than or equal to the average grayscale value (T_1), the buffer value (B_{uff}) is updated to the current pixel value. The result of the reflective noise reduction is displayed using Matplotlib, with the original and result images shown side by side in Fig-3.

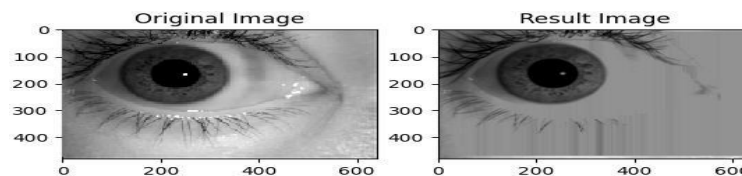


Fig-3: Noise Reduction

(b). *Iris Localization*: In Eye Images using Hough Circles and Gaussian Blur carries out the iris localization using Daugman's integro-differential operator. To make processing easier, the incoming image is first transformed to grayscale. The image is then subjected to Gaussian blur to improve feature recognition and lower noise. To find circular patterns in the image, the Hough Circles function is used. The minimum and maximum radius of circles to look for, as well as the step size for radius modification, are the important parameters for this function. $dp=1$, $minDist=5$, $minDist=5$, $param1=70$, $param1=70$, $param2=50$, $param2=50$, $minRadius=min_radius$, $maxRadius=max_radius$, particularly useful in locating the iris and pupil regions in eye images. (Daugman, 2004) Visualization of Detected Circles: If circles are detected, draw the circles on the original image with specified colors. The outer circle is drawn in green, and the center of the circle is marked in red. Result Display: Display the original and result images Fig-4 side by side using Matplotlib.

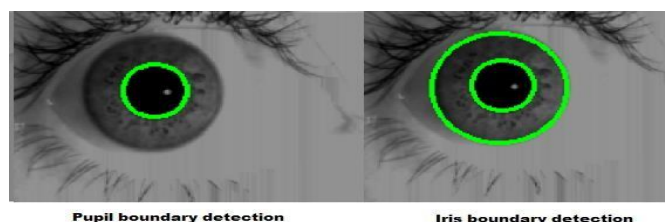


Fig-4: Pupil and Iris Localization

(c). *Segmentation*: The Hough Circles algorithm is used to identify circular objects in the picture, focusing on the iris and pupil. To attain precise detection, the HoughCircles function's parameters are adjusted. A binary mask is made to isolate the iris-corresponding region if circles are found. The segmented iris with pupil is then obtained by bitwise adding the original image with this mask. (Daugman, 2004) Following the analysis of images that meet a minimum focus condition, the iris is located precisely by employing a coarse-to-fine technique to locate its borders. This results in single-pixel accuracy estimates of the iris with pupil's centre coordinates and radius are segmented Fig-5.

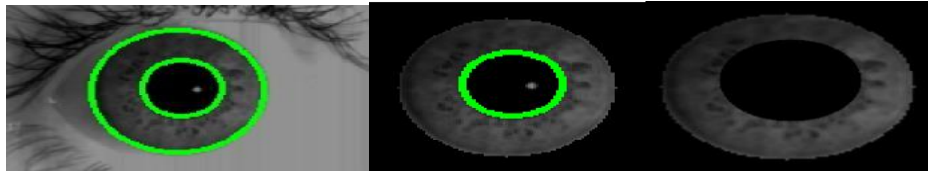


Fig-5: Segmented iris with and without pupil

(d). *Normalization*: The accuracy of the suggested method, which is based on the annular iris region to a dimensionless pseudo-polar coordinate system, is a crucial step in the conventional iris recognition method. A rectangular structure is produced because of this technique, which can be utilized to adjust for variations during crop the region of interest (International Association for Pattern Recognition et al., n.d.). The number of divisions in both radial and angular directions, as well as the inner and outer radii, is among the parameters that the code uses to create a polar coordinate grid. `np.meshgrid` is used to construct polar coordinates (theta, r). Trigonometric functions are then used to convert polar coordinates to Cartesian coordinates (x and y). To convert the original image to pseudo-polar coordinates, use the `cv2.remap` function. For easy comprehension, the original image is shown next to the image Fig-6 that has been mapped to pseudo-polar coordinates. This technique makes it possible to encode iris information efficiently in a dimensionless pseudo-polar coordinate system, which could be useful for feature extraction.

(e). *ROI*: Upon the completion of the normalization process, the Region of Interest (ROI) underwent cropping based on the gallbladder region within the right iris, as depicted in Figure-7 of the iris map. The gallbladder region specifically resides between 7 and 8 o'clock position in the right iris. According to textbooks, the lower lateral portion of the right iris encompasses the projection of the gallbladder. It is worth noting that the presence of minuscule, black patches may indicate a disorder in the gallbladder. Subsequently, the circular iris image was transformed into a rectangular shape of fixed dimensions, with the gallbladder region being precisely cropped from the iris (Gallbladder ROI_1988-R6, n.d.) After crop the region to highlight the part from the iris image needs to enhance the ROI.

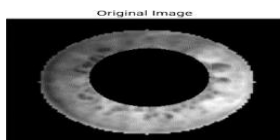


Fig-6: Normalization

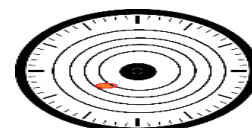


Fig-7: Position of the gallbladder in the right iris

Feature Extraction

The proposed feature extraction algorithm utilizes a Region of Interest (ROI) image as its input. To begin, the algorithm applies a one-level 2D Discrete Wavelet Transform (2D-DWT) to the ROI image, resulting in four sub-bands: cA (Approximation), cV (Vertical Detail), cD (Diagonal Detail), and cH (Horizontal Detail). Following this, features are extracted from each sub-band through statistical features, namely mean, standard deviation, skewness, kurtosis, and entropy, are computed. This set of features can then be employed for subsequent analysis and classification tasks, contributing to an effective and informative representation of the input ROI image.



Fig-8: Discrete Wavelet Transform

Statistical Features: In the analysis conducted, the impact of the number of statistical features, as well as the radial and angular resolutions, on the performance of the proposed IRS has been examined. Initially, three parameters, namely mean, median, and standard deviation, were utilized for both experiments. Subsequently, the system's performance was evaluated using six parameters: mean, median, standard deviation, skewness, kurtosis, and coefficient of variation. Additionally, the effects of radial resolution and angular resolution were also investigated. In the first experiment, the statistical features were computed along each row, resulting in a set of feature vectors (F_r) for an image. This set was then stored in the database for the identification process

$$F_r = (\bar{X}^r, Md^r, s^r, S_k^r, ku^r, CV^r), \quad r = 1, 2, 3, \dots, R \quad (1)$$

where R is the number of rows in the normalized iris picture, X_r is the row's mean, Md_r is the row's median, s_r is the row's standard deviation, S_k is the row's skewness, ku is the row's kurtosis, and CV_r is the row's co-efficient of variation. Statistical features are computed along each column in the second experiment. A set of feature vectors (F_c) for an image is obtained by this process. This collection is kept in the database for the purpose of identification. A single cropped region's evaluation value is displayed on the image Fig-9 together with its mean intensity, standard deviation, skewness, and kurtosis values.

$$F_c = (\bar{X}^c, Md^c, s^c, S_k^c, ku^c, CV^c), \quad c = 1, 2, 3, \dots, C \quad (2)$$

Mean Intensity: 131.08449074074073
 Standard Deviation: 18.318833665664542
 Skewness: -0.767607118564873
 Kurtosis: 0.4246063403400333

Fig-9: Statistical Features

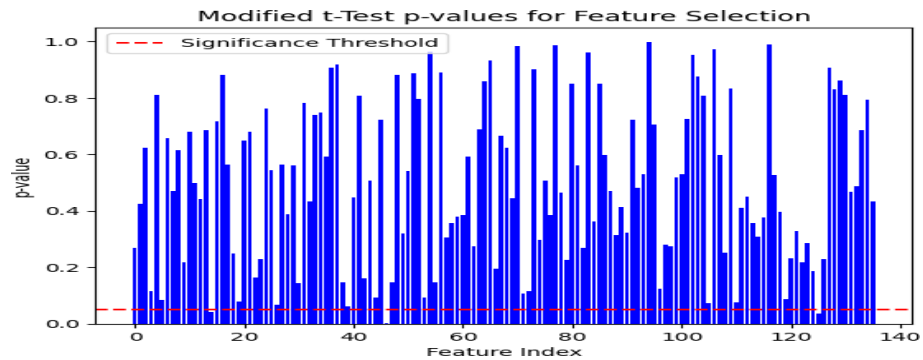


Fig-10: Modified t-test p-values for feature selection

Feature Selection

For one subject, a total of 136×1 ROI = 136 were extracted. In this study, we have explored the benefits of feature selection methods in reducing computational complexity and feature redundancy, ultimately enhancing the classification reliability. To evaluate their effectiveness in biomedical applications, we have focused on two widely used filter-based feature selection methods: the modified t test Fig-10 and ResNet50. These methods have been carefully compared and analyzed based on their computational efficiency, simplicity, and popularity. The following sections provide a detailed discussion of these feature selection methods.



Classification

The model architecture is based on the ResNet50 convolutional neural network, a widely used pre-trained model for image classification tasks. The ResNet50 base model is augmented with additional layers, including a global average pooling layer, a dense layer with rectified linear unit (ReLU) activation, a dropout layer for regularization, and a final dense layer with softmax activation to output class probabilities (Wei et al., 2022). The base ResNet50 layers are set to be non-trainable to leverage pre-trained features. The model is compiled using the Adam optimizer and categorical cross entropy loss function, with accuracy as the evaluation metric. It is then trained on the prepared dataset using the specified ImageDataGenerator for ten epochs. The output represents the training progress of a deep learning model over ten epochs using the ResNet50 architecture. Several key pieces of information are provided for each epoch: Number of Images: The training dataset consists of 2481 images belonging to two classes, indicating the utilization of pre-trained weights. Epoch-wise Training Metrics: Epoch 1/10: Loss is reported as 0.7439, and accuracy is 83.24%. Epoch 2/10: Loss decreases to 0.7795, and accuracy improves to 86.51%. Epochs 3-10: Subsequent epochs continue to report loss and accuracy metrics, showing fluctuations and trends in the model's learning. Results: Loss: The loss metric represents how well the model is performing. A decreasing loss indicates that the model is learning to make better predictions on the training data. Accuracy: The accuracy metric measures the proportion of correctly classified instances. In this case, accuracy starts at 83.24% in the first epoch and improves to 89.29% by the tenth epoch.

Conclusion

The model's learning process from the feature vector value is made clear throughout the training phase. The model appears to be adjusting to the training data throughout the course of the ten epochs, based on the shifting loss and accuracy numbers. It is important to remember that the accuracy that has been attained could still be optimized by adjusting hyper parameters, adding more data, or improving the model's architecture. Furthermore, the use of transfer learning—which makes use of information gleaned from a model trained on an alternative task or dataset—is shown by the pre-trained ResNet50 weights. Although the findings that are shown shed light on the model's performance during training, a different validation or test dataset would need to be used to fully evaluate the model's efficacy. For the model to show resilience and generalization to new data, more investigation and refinement are necessary.

References

1. Alghazo, J., & Latif, G. (2023). AI/ML-Based Medical Image Processing and Analysis. *Diagnostics*, 13(24), 3671. <https://doi.org/10.3390/diagnostics13243671>
2. Bansal, A., Agarwal, R., & Sharma, R. K. (2016). Statistical feature extraction based iris recognition system. *Sadhana - Academy Proceedings in Engineering Sciences*, 41(5), 507–518. <https://doi.org/10.1007/s12046-016-0492-9>
3. Carrera, E. V., & Maya, J. (2019). Computer aided diagnosis of gastrointestinal diseases based on iridology. *Communications in Computer and Information Science*, 895, 531–541. https://doi.org/10.1007/978-3-030-05532-5_40
4. Daugman, J. (2004). How Iris Recognition Works. *IEEE Transactions on Circuits and Systems for Video Technology*, 14(1), 21–30. <https://doi.org/10.1109/TCSVT.2003.818350>
5. Divya, C. D., Gururaj, H. L., Rohan, R., Bhagyalakshmi, V., Rashmi, H. A., Domnick, A., & Flammini, F. (2021). An efficient machine learning approach to nephrology through iris recognition. *Discover Artificial Intelligence*, 1(1). <https://doi.org/10.1007/s44163-021-00010-4>
6. *gallbladder ROI_1988-R6*. (n.d.).
7. Hussein, S. E., Hassan, O. A., & Granat, M. H. (2013). Assessment of the potential iridology for diagnosing kidney disease using wavelet analysis and neural networks. *Biomedical Signal Processing and Control*, 8(6), 534–541. <https://doi.org/10.1016/j.bspc.2013.04.006>
8. International Association for Pattern Recognition, International Association for Pattern Recognition Technical Committee on Biometrics, IEEE Biometrics Council, International Conference on Biometrics 8 2015.05.19-22 Phuket, ICB 8 2015.05.19-22 Phuket, & IAPR International Conference on Biometrics 8 2015.05.19-22 Phuket. (n.d.). *2015 International Conference on Biometrics (ICB) 19-22 May 2015, Phuket, Thailand*.
9. *IriShield™ MK2120UL*. (2021). www.iritech.com
10. Jensen, B. (1980). *IRIDOLOGY SIMPLIFIED*.
11. Lam, R., Zakko, A., Petrov, J. C., Kumar, P., Duffy, A. J., & Muniraj, T. (2021). Gallbladder Disorders: A Comprehensive Review. *Disease-a-Month*, 67(7). <https://doi.org/10.1016/j.disamonth.2021.101130>
12. Lee, E. C., & Park, K. R. (2010). Fake iris detection based on 3D structure of iris pattern. *International Journal of Imaging Systems and Technology*, 20(2), 162–166. <https://doi.org/10.1002/ima.20227>
13. Obaid, A. M., Turki, A., Bellaaj, H., Ksantini, M., AlTae, A., & Alaerjan, A. (2023). Detection of Gallbladder Disease Types Using Deep Learning: An Informative Medical Method. *Diagnostics*, 13(10). <https://doi.org/10.3390/diagnostics13101744>
14. Samant, P., & Agarwal, R. (2018a). Comparative analysis of classification based algorithms for diabetes diagnosis using iris images. *Journal of Medical Engineering and Technology*, 42(1), 35–42. <https://doi.org/10.1080/03091902.2017.1412521>
15. Samant, P., & Agarwal, R. (2018b). Machine learning techniques for medical diagnosis of diabetes using iris images. *Computer Methods and Programs in Biomedicine*, 157, 121–128. <https://doi.org/10.1016/j.cmpb.2018.01.004>
16. Tania Weidan Yu EECS, by S. (2018). *Iris Imaging for Health Diagnostics*.
17. Velia, D., & Saputro, A. H. (2020, November 10). Designing Diabetes Mellitus Detection System Based on Iridology with Convolutional Neural Network Modeling. *ICICoS 2020 - Proceeding: 4th International Conference on Informatics and Computational Sciences*. <https://doi.org/10.1109/ICICoS51170.2020.9299081>
18. Wei, Y., Zeng, A., Zhang, X., & Huang, H. (2022). RAG-Net: ResNet-50 attention gate network for accurate iris segmentation. *IET Image*



Processing, 16(11), 3057–3066. <https://doi.org/10.1049/ipr2.12538>

19. Yow, S. C., & Ali, A. N. (2019). Iris Recognition System (IRS) Using Deep Learning Technique. *Journal of Engineering Science*, 15(2), 125–144. <https://doi.org/10.21315/jes2019.15.2.9>

20. Yu, J., Zhang, L., & Wang, Z. (2021). Iris Localization Algorithm based on Effective Area. *International Journal of Antennas and Propagation*, 2021. <https://doi.org/10.1155/2021/2049646>

21. Sandhiya, M., and A. S. Aneetha. "A Survey of Advanced Learning Techniques Used for Initial Detection of vital Human organs Disorders through Iris." In *2023 9th International Conference on Smart Structures and Systems (ICSSS)*, pp. 1-4. IEEE, 2023.